Published in final edited form as:
J Struct Biol. 2014 October ; 188(1): 55–60. doi:10.1016/j.jsb.2014.08.005.

Nanoscale Three-Dimensional Imaging of the Human Myocyte

Matthew S. Sulkin[a], **Fei Yang**[b], **Katherine M. Holzem**[a], **Brandon Van Leer**[c], **Cliff Bugge**[c], **Jacob I. Laughner**[a], **Karen Green**[d], and **Igor R. Efimov**[a]

[a]Department of Biomedical Engineering, Washington University in St. Louis, MO, USA

[b]Department of Radiation Oncology, School of Medicine, Washington University in St. Louis, MO, USA

[c]FEI Company, Hillsboro, Oregon, USA

[d]Department of Pathology and Immunology, School of Medicine, Washington University in St. Louis, MO, USA

Abstract

The ventricular human myocyte is spatially organized for optimal ATP and Ca^{2+} delivery to sarcomeric myosin and ionic pumps during every excitation-contraction cycle. Comprehension of three-dimensional geometry of the tightly packed ultrastructure has been derived from discontinuous two-dimensional images, but has never been precisely reconstructed or analyzed in human myocardium. Using a focused ion beam scanning electron microscope, we created nanoscale resolution serial images to quantify the three-dimensional ultrastructure of a human left ventricular myocyte. Transverse tubules (t-tubule), lipid droplets, A-bands, and mitochondria occupy 1.8, 1.9, 10.8, and 27.9% of the myocyte volume, respectively. The complex t-tubule system has a small tortuosity (1.04 ± 0.01), and is composed of long transverse segments with diameters of 317 ± 24 nm and short branches. Our data indicates that lipid droplets located well beneath the sarcolemma are proximal to t-tubules, where 59% (13 of 22) of lipid droplet centroids are within 0.50 μm of a t-tubule. This spatial association could have an important implication in the development and treatment of heart failure because it connects two independently known pathophysiological alterations, a substrate switch from fatty acids to glucose and t-tubular derangement.

Keywords

Myocyte; Ultrastructure; Metabolism; Focused Ion Beam Tomography

Corresponding author: Igor R. Efimov, Department of Biomedical Engineering, Washington University in Saint Louis, 390E Whitaker Hall, One Brookings Drive, St. Louis, Missouri 63130-4899, Tel: 1-314-935-8612; Fax: 1-314-935-8377; igor@wustl.edu.

Disclosures:
None

Introduction

The ventricular human myocyte is uniquely optimized for hard labor without interruption for the entire lifespan of man. The densely packed ultrastructure consisting primarily of sarcomeres, mitochondria, transverse tubules (t-tubules), sarcoplasmic reticulum (SR), and lipid droplets is spatially organized to optimize ATP and Ca^{2+} delivery for contraction and relaxation. Mitochondria are proximal to both sarcomeres and SR Ca^{2+} pumps to reduce ATP diffusion length, while SR networks are adjacent to sarcomeres to accelerate delivery of Ca^{2+} to contractile proteins. T-tubules serve for three-dimensional spatiotemporal synchronization between electrical and calcium signaling, however, their role in metabolic synchronization in cardiac tissue is unknown.

Continuous progress has been made to improve the quality of electron microscope images of cardiac ultrastructure since the first attempts (Beams et al., 1949; Kisch, 1951; Kisch and Bardet, 1951; Kisch and Philpott, 1953; Kisch et al., 1948; Van Breemen, 1952; Van Breemen, 1953), and recently three-dimensional visualization techniques have been utilized to further pursue structure-function relationships (Hayashi et al., 2009; Merchan-Perez et al., 2013; Yu et al., 2008). Quantitative analysis of cardiomyocyte ultrastructure has been extensively described in mouse (Herbener, 1976; Herbener et al., 1973; Kainulainen et al., 1979; Schaper et al., 1985; Tate and Herbener, 1976), rat (Craft-Cormney and Hansen, 1980; Guski et al., 1981; Laguens, 1971; Lund and Tomanek, 1978; Lund and Tomanek, 1980; Page et al., 1974; Reith and Fuchs, 1973; Schaper et al., 1985; Tomanek and Hovanec, 1981; Tomanek et al., 1979), and canine hearts (Becker et al., 1999; Gerdes and Kasten, 1980; Goldstein and Murphy, 1983; McCallister et al., 1978; Papadimitriou et al., 1974; Partin et al., 1972; Schaper et al., 1985), while fewer studies have investigated ultrastructure morphology of human cardiomyocytes (Fleischer et al., 1980; Laguens et al., 1979; Schaper et al., 1985).

Here, we utilize a dual-beam electron microscope for the first time in healthy human left ventricular (LV) tissue to create high-resolution serial images at nanometer resolution for three-dimensional analysis. Our morphometric results, including ultrastructure volume and t-tubule geometry compare nicely to previous reports in mammalian ventricular myocytes. Further analyses indicate a novel finding—lipid droplets well beneath the sarcolemma are spatially located near t-tubules. The observed spatial association was compared against simulations that randomly placed lipid droplets within the volume and showed that the experimentally observed proximity could not be repeated.

Material and Methods

Tissue Collection

The study was approved by the Washington University Institutional Review Board. A non-failing donor heart was provided by Mid-America Transplant Services (Saint Louis, MO). The donor was a 55 year old female with a history of hypertension and the cause of death was cerebral hypoxia. The heart was arrested with cardioplegic solution (110 NaCl, 1.2 $CaCl_2$, 16 KCl, 16 $MgCl_2$, 10 $NaHCO_3$ mmol/L) and explanted for experimentation. The donor heart was transported to the laboratory in cold (~4°C) cardioplegic solution in 15

minutes. A transverse sample (~150 μm thick) of apical-posterior left ventricle was collected (Anchor, Soft Tissue Biopsy Device, Addison, IL) and both epicardial fat and papillary muscle were discarded.

Tissue Fixation and Embedding

Excised tissue was immediately immersion fixed in a modified Karnovsky's fixative (3% glutaraldehyde, 1% paraformaldehyde in 0.1M sodium cacodylate buffer), post-fixed in cacodylate buffered 2% osmium tetroxide, dehydrated in graded ethanols and propylene oxide, and embedded in EMBed-812 resin (Electron Microscopy Sciences, Hatfield, PA).

Focused Ion Beam-Scanning Electron Microscopy

After tissue embedding, serial images were obtained using a Helios NanoLab 650 DualBeam microscope (FEI, Hillsboro, Oregon). A 30 keV Ga^+ focused ion beam (FIB) was directed parallel to the LV tissue block for removing (milling) thin layers (10 nm), while a 2 keV scanning electron probe was employed for imaging. Images were acquired in backscatter mode using the Through-the-Lens detector. Automated milling and imaging of the LV block face provided 220 images (Auto Slice & View, FEI) with high resolution (4096 × 3536, voxel dimension 3.6 nm × 4.2 nm × 10 nm) to allow for the identification of t-tubules, lipid droplets, mitochondrial networks, A-bands, and sarcolemma throughout the entire ~15 μm × 15 μm × 2.2 μm volume.

Segmentation

Various ad hoc segmentation techniques were applied to reconstruct the two-dimensional images into three-dimension volumes. Boundaries of lipid droplets and sarcolemma were defined using automatic thresholding combined with edge detection. T-tubules and A-bands were contoured with active contour followed by morphological operations. Due to their heterogeneic, complex shape mitochondrial networks were delineated manually. Once the features of interest were defined and segmented, polygonal surface models of the structures were created using Avizo software (Visualization Sciences Group, Burlington, MA).

Ultrastructure Analysis

Analysis was implemented using MATLAB (MathWorks, Natick, MA) software we wrote. Only ultrastructure within the cardiac myocyte was considered. Percent volume was calculated for t-tubules, A-bands, lipid droplets, and mitochondria. The distance between lipid droplets and other ultrastructure was approximated as the distance between droplet centroids to the nearest ultrastructure surface. The observed spatial distribution between lipid droplets (n=31) and ultrastructure was compared to a simulation that randomly placed lipid droplets (n=31) within the volume. The simulation was performed 10 times. T-tubule tortuosity, diameter, and cross sectional area were calculated. Tortuosity was estimated as the total t-tubule length divided by the Euclidean distance from opposite ends of the t-tubules ($L_{Total}/L_{Euclidean}$). T-tubule diameter and cross sectional area were calculated from n=440 samples and are expressed as the mean ± standard deviation.

Results and Discussion

Segmentation

Figure 1A displays the donated heart with the location of the apical-posterior sample emphasized by a black asterisk. White dotted lines in Figure 1B highlight ultrastructure, which can be identified throughout the serial section volume (Figure 1C). Using various image-processing techniques, we were able to accurately segment the ultrastructure of the myocyte. Figure 1D displays the two-dimensional segmentation of the A-bands (green), lipid droplets (yellow), and mitochondria (red), from the first image of the serial section volume.

Volume Reconstruction

Three-dimension reconstruction of the t-tubules (purple), lipid droplets (yellow), A-bands (green), and mitochondria (red), are shown in Figure 2 and 3. In Figure 2, the reconstructed volumes are individually shown inside the serial section bounding box, with the bottom serial image and edges displayed. T-tubules and lipid droplets are seen throughout the volume, while mitochondria form their distinct subsarcolemmal and intermyofibrillar subpopulations. T-tubules, lipid droplets, A-bands, and mitochondria occupy 1.8, 1.9, 10.8, and 27.9% of the myocyte volume, respectively.

In Figure 3, the serial section volume provides orientation for the reconstructed ultrastructure below. As their name suggests, t-tubules predominately orient transversely to the longitudinal axis of the myocyte, yet longitudinal extensions exist. Alternative names, such as sarcolemmal tubule network (Sommer and Jennings, 1992), transverse-axial tubular system (Forbes et al., 1984), and sarcolemmal Z rete (Soeller and Cannell, 1999) have been suggested as more appropriate names. The calculated tortuosity of the t-tubular network is 1.04 ± 0.01 (straight line = 1.0). This indicates that t-tubules have predominately long straight segments and short curved branching segments. T-tubule diameter and cross-sectional area are 317 ± 24 nm and 8,640 ± 1,800 nm^2, respectively. This diameter is greater than the 255 nm diameter reported for rat ventricular myocytes (Soeller and Cannell, 1999), but is within the range (20–450 nm) typically given for individual t-tubules (Brette and Orchard, 2003). The compactness of the ultrastructure is clearly seen in Figure 3-Bottom, where intermyofibrillar mitochondria align between A-bands and lipid droplets are enveloped by mitochondria.

Lipid Droplet and Ultrastructure Association

In Figure 4, the mitochondria and A-bands are omitted from the three-dimensional reconstruction to visualize the spatial localization of lipid droplets with respect to the sarcolemma (teal) and t-tubules (purple). In Figure 4A, the sarcolemma has been thickened (≈100×) to enhance its visibility. In Figure 4A-Left, the sarcolemma is displayed only with lipid droplets, which appear to be randomly placed in the volume. However, when t-tubules are reintroduced into the volume (Figure 4A-Middle, Right) lipid droplets located well beneath the sarcolemma appear to be co-localized with t-tubules. Black boxes in Figure 4A highlight lipid droplets proximal to t-tubules, while brown boxes highlight lipid droplets situated adjacent to the sarcolemma. The Online Supplemental Movie rotates lipid droplet

and t-tubule volumes inside the 220 serial sections 360-degrees, which is optimal for visualization of the reconstructed ultrastructure.

The distance between lipid droplets and ultrastructure was calculated for both experimentally observed and simulated conditions to determine whether a spatial association exists. All experimentally observed lipid droplets were within 0.50 μm (red, Figure 4B) of a mitochondria. Likewise, when lipid droplets were randomly placed in the volume all lipid droplets (n=310) were within 0.50 μm of a mitochondrion. A representative simulated distribution (grey, n=31 lipid droplets) is displayed in Figure 4B. The high density of mitochondria in the myocyte ensures lipid droplets will be nearby.

The distribution of the distances between lipid droplets and t-tubules is displayed in Figure 4C, where the dashed black line highlights the average midpoint between t-tubules (1.25 μm). Out of 31 experimentally observed lipid droplets, 42% (13 of 31) are within 0.50 μm of a t-tubule (purple). When lipid droplets are randomly placed in the volume, however, only 21% (64 of 310) are within 0.50 μm of a t-tubule. A representative simulated distribution (grey, n=31 lipid droplets) is shown in Figure 4C. Overall, 29% of the experimentally observed lipid droplets (9 of 31) are located proximal the sarcolemma and 71% (22 of 31) are located between myofibrils. If only intermyofibrillar lipid droplets are considered, 59% (13 of 22) are within 0.50 μm of a t-tubule. This proximity was never seen in the simulations. Out of the 10 experimentally observed lipid droplets that are located farther than the midpoint (right of dashed line), 7 are adjacent (<0.50 μm) to the sarcolemma. Thus, the overwhelming majority of lipid droplets are proximal to the sarcolemma or t-tubules.

In healthy adult myocardium, approximately 60–70% of ATP is generated by oxidation of fatty acids (Huss and Kelly, 2005), requiring an organized and efficient system to continuously supply mitochondria with fatty acids. In rodent hearts, it was shown that perilipin 5 provides a physical link between lipid droplets and mitochondria through a C-terminal region (Wang et al., 2011), however the mechanism of the accumulation of lipid droplets proximal to intermyofibrillar mitochondria is unknown. We speculate that fatty acid transporters, such as fatty acid translocase/CD36 are concentrated at t-tubules, similar to calcium handling proteins (Brette and Orchard, 2003), and aid in fatty acid delivery deep into the myocyte. Alternatively t-tubules may provide a structural scaffold that enable lipid droplets to move into the interior of the cell. This spatial relationship would have important implications for myocardium in heart failure because it mechanistically links two distinctly different observations made during the progression of heart failure: (1) the principle energy substrate switches from fatty acids to glucose (Huss and Kelly, 2005; Osorio et al., 2002; Razeghi et al., 2001; Sack et al., 1996) and (2) t-tubular derangement (Ibrahim et al., 2012; Lyon et al., 2009; Wei et al., 2010).

The metabolic switch to glucose utilization with the progression of heart failure has led investigators to pharmacologically modulate fatty acid oxidation with the expectation of being therapeutically beneficial. Despite some inconsistent reports, the majority of studies have shown that the direct or indirect improvement of fatty acid supply during heart failure has minimal functional benefits (Halbirk et al., 2010; Labinskyy et al., 2007; Lionetti et al., 2011; Morgan et al., 2006), while increased carbohydrate oxidation has been shown to

enhance LV function in animal and short term clinical studies (3–6 months) (Abozguia et al., 2010; Fragasso et al., 2008; Fragasso et al., 2006a; Fragasso et al., 2006b; Lee et al., 2005; Lionetti et al., 2011). Structurally intact t-tubules may be required for efficient delivery of fatty acids or lipid droplets well beneath the sarcolemma and their remodeling during heart failure could inhibit fatty acid oxidations therapeutic benefit.

Conclusion

FIB scanning electron microscopy produced serial images of a human LV myocyte at nanoscale resolution enabling segmentation and volume reconstruction of ultrastructure. Detailed morphometric analysis was performed on a single 3D data set. Analysis showed that lipid droplets located well beneath the sarcolemma are proximal to t-tubules, which could implicate a role for t-tubules in the efficient delivery of lipid droplets to intermyofibrillar mitochondria.

Supplementary Material

Refer to Web version on PubMed Central for supplementary material.

Acknowledgments

Funding:

This research was supported by NIH/NHLBI grant R01 HL114395.

Abbreviations

T-tubules	Transverse tubules
SR	Sarcoplasmic reticulum
LV	Left ventricle
FIB	Focused ion beam

References

Abozguia K, Elliott P, McKenna W, Phan TT, Nallur-Shivu G, Ahmed I, Maher AR, Kaur K, Taylor J, Henning A, Ashrafian H, Watkins H, Frenneaux M. Metabolic modulator perhexiline corrects energy deficiency and improves exercise capacity in symptomatic hypertrophic cardiomyopathy. Circulation. 2010; 122:1562–1569. [PubMed: 20921440]

Beams HW, Evans TC, et al. Electron microscope studies on the structure of cardiac muscle. The Anatomical record. 1949; 105:59–81. incl 53 pl. [PubMed: 15393666]

Becker LC, Jeremy RW, Schaper J, Schaper W. Ultrastructural assessment of myocardial necrosis occurring during ischemia and 3-h reperfusion in the dog. The American journal of physiology. 1999; 277:H243–252. [PubMed: 10409203]

Brette F, Orchard C. T-tubule function in mammalian cardiac myocytes. Circulation research. 2003; 92:1182–1192. [PubMed: 12805236]

Craft-Cormney C, Hansen JT. Early ultrastructural changes in the myocardium following thyroxine-induced hypertrophy. Virchows Archiv B, Cell pathology including molecular pathology. 1980; 33:267–273.

Fleischer M, Wippo W, Themann H, Achatzy RS. Ultrastructural morphometric analysis of human myocardial left ventricles with mitral insufficiency. A comparison with normally loaded and hypertrophied human left ventricles. Virchows Archiv A, Pathological anatomy and histology. 1980; 389:205–210.

Forbes MS, Hawkey LA, Sperelakis N. The transverse-axial tubular system (TATS) of mouse myocardium: its morphology in the developing and adult animal. The American journal of anatomy. 1984; 170:143–162. [PubMed: 6465048]

Fragasso G, Salerno A, Spoladore R, Bassanelli G, Arioli F, Margonato A. Metabolic therapy of heart failure. Current pharmaceutical design. 2008; 14:2582–2591. [PubMed: 18991675]

Fragasso G, Palloshi A, Puccetti P, Silipigni C, Rossodivita A, Pala M, Calori G, Alfieri O, Margonato A. A randomized clinical trial of trimetazidine, a partial free fatty acid oxidation inhibitor, in patients with heart failure. Journal of the American College of Cardiology. 2006a; 48:992–998. [PubMed: 16949492]

Fragasso G, Perseghin G, De Cobelli F, Esposito A, Palloshi A, Lattuada G, Scifo P, Calori G, Del Maschio A, Margonato A. Effects of metabolic modulation by trimetazidine on left ventricular function and phosphocreatine/adenosine triphosphate ratio in patients with heart failure. European heart journal. 2006b; 27:942–948. [PubMed: 16510466]

Gerdes AM, Kasten FH. Morphometric study of endomyocardium and epimyocardium of the left ventricle in adult dogs. The American journal of anatomy. 1980; 159:389–394. [PubMed: 7223674]

Goldstein MA, Murphy DL. A morphometric analysis of ischemic canine myocardium with and without reperfusion. Journal of molecular and cellular cardiology. 1983; 15:325–334. [PubMed: 6887262]

Guski H, Meerson FZ, Wassilew G. Comparative study of ultrastructure and function of the rat heart hypertrophied by exercise or hypoxia. Experimental pathology. 1981; 20:108–120. [PubMed: 6459951]

Halbirk M, Norrelund H, Moller N, Schmitz O, Gotzsche L, Nielsen R, Nielsen-Kudsk JE, Nielsen SS, Nielsen TT, Eiskjaer H, Botker HE, Wiggers H. Suppression of circulating free fatty acids with acipimox in chronic heart failure patients changes whole body metabolism but does not affect cardiac function. American journal of physiology Heart and circulatory physiology. 2010; 299:H1220–1225. [PubMed: 20709866]

Hayashi T, Martone ME, Yu Z, Thor A, Doi M, Holst MJ, Ellisman MH, Hoshijima M. Three-dimensional electron microscopy reveals new details of membrane systems for Ca2+ signaling in the heart. Journal of cell science. 2009; 122:1005–1013. [PubMed: 19295127]

Herbener GH. A morphometric study of age-dependent changes in mitochondrial population of mouse liver and heart. Journal of gerontology. 1976; 31:8–12. [PubMed: 1244408]

Herbener GH, Swigart RH, Lang CA. Morphometric comparison of the mitochondrial populations of normal and hypertrophic hearts. Laboratory investigation; a journal of technical methods and pathology. 1973; 28:96–103.

Huss JM, Kelly DP. Mitochondrial energy metabolism in heart failure: a question of balance. The Journal of clinical investigation. 2005; 115:547–555. [PubMed: 15765136]

Ibrahim M, Navaratnarajah M, Siedlecka U, Rao C, Dias P, Moshkov AV, Gorelik J, Yacoub MH, Terracciano CM. Mechanical unloading reverses transverse tubule remodelling and normalizes local Ca(2+)-induced Ca(2+)release in a rodent model of heart failure. European journal of heart failure. 2012; 14:571–580. [PubMed: 22467752]

Kainulainen H, Pilstrom L, Vihko V. Morphometry of myocardial apex in endurance-trained mice of different ages. Acta physiologica Scandinavica. 1979; 107:102–114. [PubMed: 525372]

Kisch B. Physiological aspects of electron microscopy of the heart. Experimental medicine and surgery. 1951; 9:333–373. [PubMed: 14860200]

Kisch B, Bardet JM. Electron-histology of the heart elements of the heart and blood of the mouse. Experimental medicine and surgery. 1951; 9:1–47. [PubMed: 14813266]

Kisch B, Philpott DE. Electron-microscopic investigations of the human heart. Experimental medicine and surgery. 1953; 11:161–173. [PubMed: 13117032]

Kisch B, Grey CE, Kelsch JJ. Electron histology of the heart. Experimental medicine and surgery. 1948; 6:346–365. [PubMed: 18104765]

Labinskyy V, Bellomo M, Chandler MP, Young ME, Lionetti V, Qanud K, Bigazzi F, Sampietro T, Stanley WC, Recchia FA. Chronic activation of peroxisome proliferator-activated receptor-alpha with fenofibrate prevents alterations in cardiac metabolic phenotype without changing the onset of decompensation in pacing-induced heart failure. The Journal of pharmacology and experimental therapeutics. 2007; 321:165–171. [PubMed: 17215446]

Laguens R. Morphometric study of myocardial mitochondria in the rat. The Journal of cell biology. 1971; 48:673–676. [PubMed: 5545333]

Laguens RP, Weinschelbaun R, Favaloro R. Ultrastructural and morphometric study of the human heart muscle cell in acute coronary insufficiency. Human pathology. 1979; 10:695–705. [PubMed: 527966]

Lee L, Campbell R, Scheuermann-Freestone M, Taylor R, Gunaruwan P, Williams L, Ashrafian H, Horowitz J, Fraser AG, Clarke K, Frenneaux M. Metabolic modulation with perhexiline in chronic heart failure: a randomized, controlled trial of short-term use of a novel treatment. Circulation. 2005; 112:3280–3288. [PubMed: 16301359]

Lionetti V, Stanley WC, Recchia FA. Modulating fatty acid oxidation in heart failure. Cardiovascular research. 2011; 90:202–209. [PubMed: 21289012]

Lund DD, Tomanek RJ. Myocardial morphology in spontaneously hypertensive and aortic-constricted rats. The American journal of anatomy. 1978; 152:141–151. [PubMed: 150224]

Lund DD, Tomanek RJ. The effects of chronic hypoxia on the myocardial cell of normotensive and hypertensive rats. The Anatomical record. 1980; 196:421–430. [PubMed: 6446867]

Lyon AR, MacLeod KT, Zhang Y, Garcia E, Kanda GK, Lab MJ, Korchev YE, Harding SE, Gorelik J. Loss of T-tubules and other changes to surface topography in ventricular myocytes from failing human and rat heart. Proceedings of the National Academy of Sciences of the United States of America. 2009; 106:6854–6859. [PubMed: 19342485]

McCallister LP, Daiello DC, Tyers GF. Morphometric observations of the effects of normothermic ischemic arrest on dog myocardial ultrastructure. Journal of molecular and cellular cardiology. 1978; 10:67–80. [PubMed: 621742]

Merchan-Perez A, Rodriguez JR, Gonzalez S, Robles V, Defelipe J, Larranaga P, Bielza C. Three-Dimensional Spatial Distribution of Synapses in the Neocortex: A Dual-Beam Electron Microscopy Study. Cerebral cortex (New York, NY : 1991). 2013

Morgan EE, Rennison JH, Young ME, McElfresh TA, Kung TA, Tserng KY, Hoit BD, Stanley WC, Chandler MP. Effects of chronic activation of peroxisome proliferator-activated receptor-alpha or high-fat feeding in a rat infarct model of heart failure. American journal of physiology Heart and circulatory physiology. 2006; 290:H1899–1904. [PubMed: 16339830]

Osorio JC, Stanley WC, Linke A, Castellari M, Diep QN, Panchal AR, Hintze TH, Lopaschuk GD, Recchia FA. Impaired myocardial fatty acid oxidation and reduced protein expression of retinoid X receptor-alpha in pacing-induced heart failure. Circulation. 2002; 106:606–612. [PubMed: 12147544]

Page E, Earley J, Power B. Normal growth of ultrastructures in rat left ventricular myocardial cells. Circulation research. 1974; 35(suppl II):12–16. [PubMed: 4843570]

Papadimitriou JM, Hopkins BE, Taylor RR. Regression of left ventricular dilation and hypertrophy after removal of volume overload. Morphological and ultrastructural study. Circulation research. 1974; 35:127–135. [PubMed: 4276275]

Partin JS, Benzing G 3rd, Partin JC. Quantitative fine structural changes in dog heart following cardiopulmonary bypass. Journal of molecular and cellular cardiology. 1972; 4:345–355. [PubMed: 5052590]

Razeghi P, Young ME, Alcorn JL, Moravec CS, Frazier OH, Taegtmeyer H. Metabolic gene expression in fetal and failing human heart. Circulation. 2001; 104:2923–2931. [PubMed: 11739307]

Reith A, Fuchs S. The heart muscle of the rat under influence of triiodothyronine and riboflavin deficiency with special reference to mitochondria. A morphologic and morphometric study by

electron microscopy. Laboratory investigation; a journal of technical methods and pathology. 1973; 29:229–235.

Sack MN, Rader TA, Park S, Bastin J, McCune SA, Kelly DP. Fatty acid oxidation enzyme gene expression is downregulated in the failing heart. Circulation. 1996; 94:2837–2842. [PubMed: 8941110]

Schaper J, Meiser E, Stammler G. Ultrastructural morphometric analysis of myocardium from dogs, rats, hamsters, mice, and from human hearts. Circulation research. 1985; 56:377–391. [PubMed: 3882260]

Soeller C, Cannell MB. Examination of the transverse tubular system in living cardiac rat myocytes by 2-photon microscopy and digital image-processing techniques. Circulation research. 1999; 84:266–275. [PubMed: 10024300]

Sommer, JR.; Jennings, RB. Ultrastructure of Cardiac Muscle. In: Fozzard, HA., et al., editors. The Heart and Cardiovascular System. Raven Press, Ltd; New York: 1992.

Tate EL, Herbener GH. A morphometric study of the density of mitochondrial cristae in heart and liver of aging mice. Journal of gerontology. 1976; 31:129–134. [PubMed: 1249400]

Tomanek RJ, Hovanec JM. The effects of long-term pressure-overload and aging on the myocardium. Journal of molecular and cellular cardiology. 1981; 13:471–488. [PubMed: 7265256]

Tomanek RJ, Davis JW, Anderson SC. The effects of alpha-methyldopa on cardiac hypertrophy in spontaneously hypertensive rats: ultrastructural, stereological, and morphometric analysis. Cardiovascular research. 1979; 13:173–182. [PubMed: 157811]

Van Breemen VL. Myofibril development observed with the electron microscope. The Anatomical record. 1952; 113:179–195. [PubMed: 14933809]

Van Breemen VL. Intercalated discs in heart muscle studied with the electron microscope. The Anatomical record. 1953; 117:49–63. [PubMed: 13092553]

Wang H, Sreenivasan U, Hu H, Saladino A, Polster BM, Lund LM, Gong DW, Stanley WC, Sztalryd C. Perilipin 5, a lipid droplet-associated protein, provides physical and metabolic linkage to mitochondria. Journal of lipid research. 2011; 52:2159–2168. [PubMed: 21885430]

Wei S, Guo A, Chen B, Kutschke W, Xie YP, Zimmerman K, Weiss RM, Anderson ME, Cheng H, Song LS. T-tubule remodeling during transition from hypertrophy to heart failure. Circulation research. 2010; 107:520–531. [PubMed: 20576937]

Yu Z, Holst MJ, Hayashi T, Bajaj CL, Ellisman MH, McCammon JA, Hoshijima M. Three-dimensional geometric modeling of membrane-bound organelles in ventricular myocytes: bridging the gap between microscopic imaging and mathematical simulation. Journal of structural biology. 2008; 164:304–313. [PubMed: 18835449]

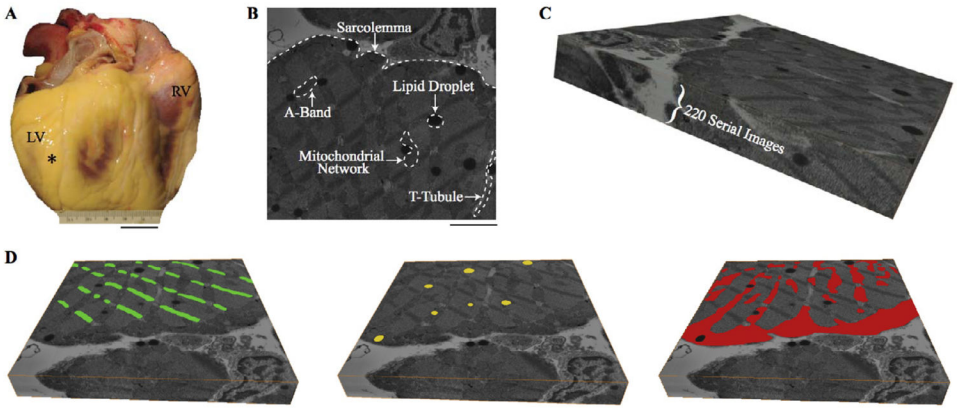

Figure 1.

Ultrastructure segmentation. **A.** Donated human heart with location of tissue sample marked by black asterisk. **B.** Example two-dimensional scanning electron microscopy image with ultrastructure highlighted. **C.** Serial section volume of 220 slices each 10 nm thick **D.** Example digital segmentation of A-bands (green), lipid droplets (yellow), and mitochondria (red) on first serial section. Scale Bars: 2 cm (A), 3 μm (B). Serial Section Volumes: 14.7 μm × 14.8 μm × 2.2 μm (C and D).

RV: right ventricle; LV: left ventricle; T-tubule: transverse tubule.

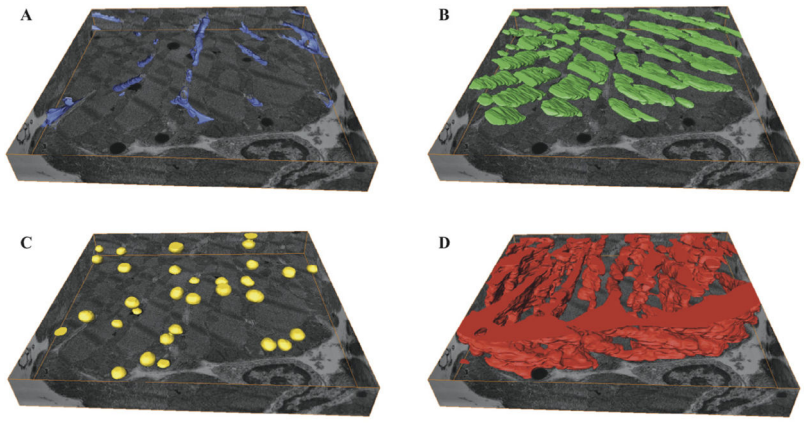

Figure 2.

Three-dimensional reconstruction of ultrastructure with bottom serial section image and edges serving as a bounding box. **A.** Transverse-tubules (purple). **B.** A-band (green). **C.** Lipid droplets (yellow) **D.** Mitochondria (red). Serial Section Volumes: 14.7 μm × 14.8 μm × 2.2 μm (A, B, C, and D).

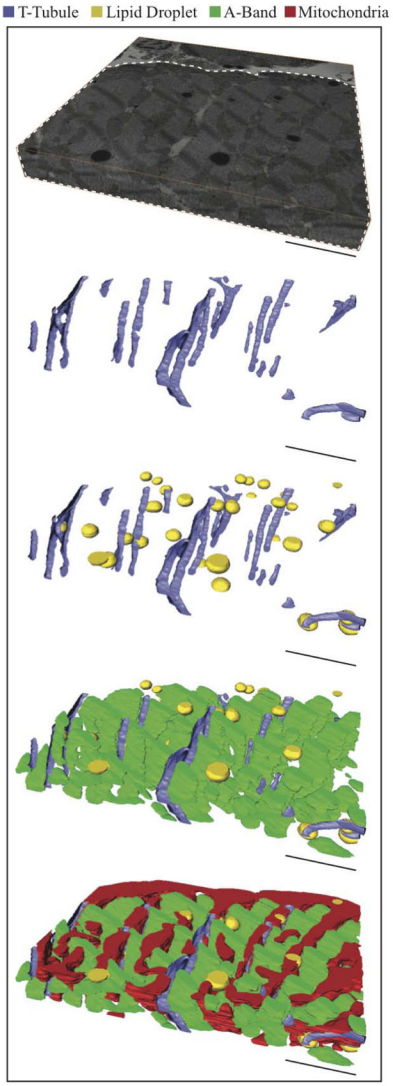

Figure 3.

Sequential addition of ultrastructure. The serial section volume (Top) shows the orientation of the reconstructed ultrastructure volumes below, where the whited dotted line highlights the area of interest (myocyte). Scale Bars: 3 μm Serial Section. Volume: 14.7 μm × 14.8 μm × 2.2 μm (Top).

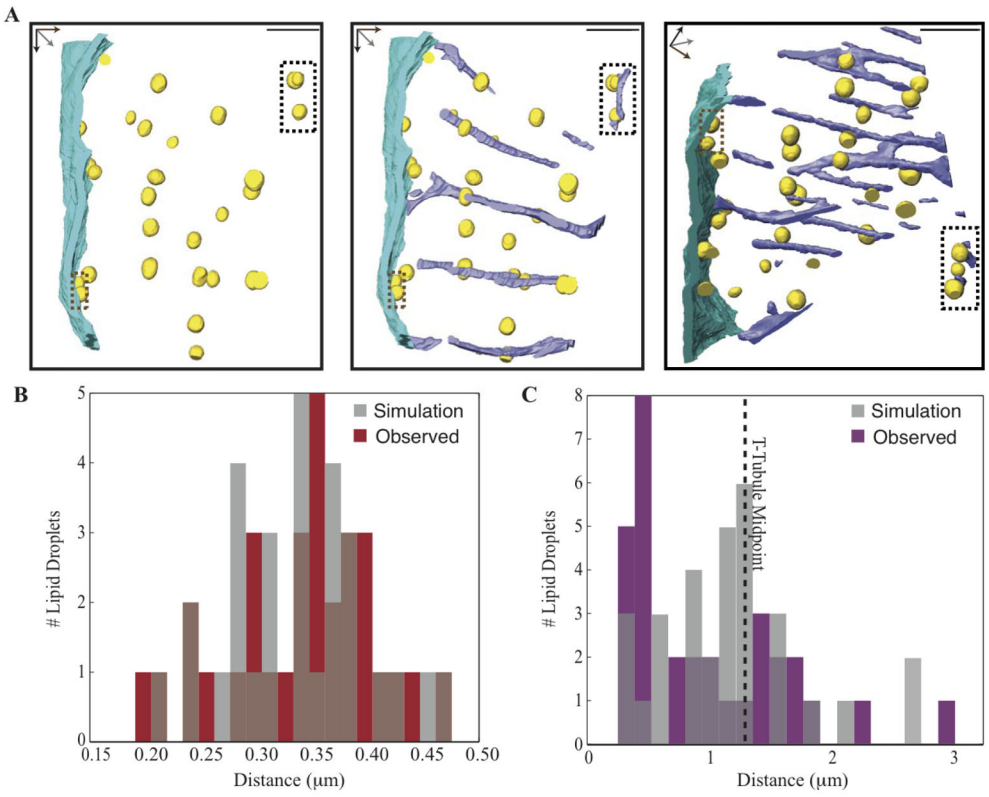

Figure 4.

Lipid droplet association with mitochondria and (t-tubules). **A.** Lipid droplets (yellow) and sarcolemma (teal) are visualized without (Left) and with (Middle, Right) t-tubules. Left and Middle panels are in the same orientation. Black and brown dotted boxes highlight lipid droplets associated with t-tubules and sarcolemma, respectively. **B.** Distribution of simulated (grey) and experimentally observed (red) distances from lipid droplet centroids to nearest mitochondria. **C.** Distribution of simulated (grey) and experimentally observed (purple) distances from lipid droplet centroids to nearest t-tubule. Scale Bars: 3 μm (A).